High Temperature Expansion and Exact Diagonalization of the Rhodium Nuclear Spin System Compared to Experimental Results

K. I. Juntunen, K. Lefmann*, T. A. Knuuttila, and J. T. Tuoriniemi

Low Temperature Laboratory, Helsinki University of Technology, P.O. Box 2200, FIN-02015 HUT, Finland
*Dept. of Materials Science, Risø National Laboratory, DK-4000, Roskilde, Denmark

The nuclear spin system of Rh metal has recently been investigated experimentally. No nuclear magnetic ordering was observed in these measurements, in spite of the very low nuclear entropy achieved. To study this system theoretically, we have applied the method of exact diagonalization to a 16 spin I=1/2 fcc cluster with both Ruderman-Kittel and dipolar interactions. In this work, we compare the results of this method with the experimental data and the high temperature expansion results in the paramagnetic state. The high temperature expansions agree with the experimental data down to 1 nK, while the exact diagonalisation results are less accurate.

1. INTRODUCTION

The physical properties of a magnetic system in the paramagnetic state are often used experimentally to extract knowledge about the system, *e.g.* the magnitude and sign of the spin-spin interactions. This is especially the case for nuclear magnets, where reaching the magnetically ordered state is extremely difficult. The work presented in this paper deals with the thermodynamic properties of the $I = 1/2$ Rh nuclear spin system, which was recently cooled to a temperature below 100 pK without observation of ordering [1], although the mean-field ordering temperature has been estimated to 1.5 nK [2]. The methods used for this study are applicable also for other spin systems.

Much effort has been put into studies of the thermodynamical prop-

K. I. Juntunen, K. Lefmann, T. A. Knuuttila, and J. T. Tuoriniemi

erties of spin systems close to the ordering temperature, T_c, to reveal the universal properties of phase transitions [3]. A powerful method that includes the effects of quantum mechanics is the $(1/T)$ high-temperature expansion (HTE) of the partition function, as deviced by van Vleck [4]. However, HTE has the drawback that it diverges for high values of $\beta \equiv 1/T$. If there is an inherent frustration in the system, the divergence typically happens above T_c. Nevertheless, HTE is the standard choice for describing nuclear spin systems at $T \gg T_c$. One way of removing the divergences of the HTE is by using Padé approximants, which we will describe later in this paper. A thorough review on the theory of nuclear spin systems is given by Ref. 2.

In the paramagnetic state close to T_c, the thermodynamics of the spin system is governed by the (short-range) correlations between the spins. One way of calculating the effect of short-range correlations is exact numerical diagonalisation (ED) of small spin clusters. ED was early used to describe the thermodynamics of the nearest neighbor (nn) $s = 1/2$ Heisenberg chain [5], and the method has later been used, *e.g.* for the nn 2D $s = 1/2$ square Heisenberg lattice [6], and for an exchange Hamiltonian in the 3D bcc lattice [7]. An important difference between ED and HTE is that the former does not diverge at any temperature. ED does, however, give unphysical results at the very lowest temperatures, due to the finite size energy gap. Further, phase transitions to truly long range ordered state are not possible in finite-sized systems, and only finite-size precursors of ordering can be found [6].

In this paper we obtain information about the thermodynamics of the Rh nuclear spin system in the paramagnetic state from a combination of HTE and ED. The validity of the HTE expressions and the Padé approximant method was checked by performing the calculations on the finite size spin systems where the exact answer is known from ED. Preliminary ED results of this work were reported earlier [8]. We compare our results with the recent experimental data, most of which are published in Ref. 1.

2. THE NUCLEAR SPIN HAMILTONIAN

The Hamiltonian for the nuclear spin system in rhodium is given by

$$H = -\gamma\hbar\mathbf{B} \cdot \sum_j \mathbf{I}_j + \frac{1}{2}\sum_{j,k} J_{jk}\mathbf{I}_j \cdot \mathbf{I}_k + H_{\mathrm{d}} + H_{\mathrm{a}}, \qquad (1)$$

where the first term is the Zeeman interaction, the second describes the conduction-electron mediated isotropic exchange, *i.e.* Ruderman-Kittel (RK) interactions, H_{d} describes the dipolar interaction, and H_{a} the d-electron mediated anisotropic exchange interactions. The anisotropic indirect interac-

tion can be approximated to be of the same form as the dipolar interaction, and we may write

$$H_{\mathrm{d}} + H_{\mathrm{a}} \;\; = \;\; \frac{1}{2} \sum_{j,k} D_{jk} \Big[\mathbf{I}_j \cdot \mathbf{I}_k - 3(\mathbf{I}_j \cdot \hat{\mathbf{r}}_{jk})(\mathbf{I}_k \cdot \hat{\mathbf{r}}_{jk}) \Big] \tag{2}$$

where $D_{jk} = \mu_0 \gamma_{\mathrm{eff}}^2 \hbar^2 / (4\pi r_{jk}^3)$ and $\hat{\mathbf{r}}_{jk}$ is a unit vector along the line connecting spin j and spin k. The effective gyromagnetic ratio for rhodium is measured as $(\gamma_{\mathrm{eff}}/\gamma)^2 = 1.4 \pm 0.1$ [9].

2.1. Calculation of the interaction parameters

The Ruderman-Kittel parameter R describes the relative magnitudes of the RK and dipolar interactions, and it is defined as

$$R = \frac{-\sum_k J_{0k}}{\mu_0 \hbar^2 \gamma^2 \rho} \;\; , \tag{3}$$

where ρ is the number density. For rhodium this has been measured to be $R_{\mathrm{Rh}} = -1.2 \pm 0.1$ [9]. The local field is a measure of the strength of the spin-spin interactions and it is defined by

$$B_{\mathrm{loc}}^2 \;\; = \;\; B_{\mathrm{RK}}^2 + B_{\mathrm{d}}^2 = \frac{I(I+1)}{2\gamma^2 \hbar^2} \sum_k J_{0k}^2 + \frac{I(I+1)}{\gamma^2 \hbar^2} \sum_k D_{0k}^2, \tag{4}$$

which has the value $B_{\mathrm{loc,Rh}} = 33 \pm 2 \; \mu\mathrm{T}$ [1]. For the nuclear spin systems of Cu and Ag, the RK interactions were determined through first-principles band structure calculations [10]. In contrast, no band structure calculations have been performed on rhodium. Thus, an alternative way of determining these is needed. The RK interaction decreases rapidly with distance, so approximate values for the nn and next nearest neighbor (nnn) interaction parameters J_{nn} and J_{nnn} can be found by ignoring all higher coupling constants and satisfying the relations (3) and (4). For rhodium, we get $J_{\mathrm{nn}} = 14.9 \; (h \; \mathrm{Hz})$ and $J_{\mathrm{nnn}} = -8.12 \; (h \; \mathrm{Hz})$, where h is Planck's constant. Also another pair of solutions exists, but this is not reasonable since for these solutions $|J_{\mathrm{nn}}| < |J_{\mathrm{nnn}}|$. The dipolar parameters used in this work were $D_{\mathrm{nn}} = 8.63 \; (h \; \mathrm{Hz})$ and $D_{\mathrm{nnn}} = 3.05 \; (h \; \mathrm{Hz})$, which include the anisotropic exchange interactions through multiplication of the pure dipolar parameters by $(\gamma_{\mathrm{eff}}/\gamma)^2$.

The calculation of J_{nn} and J_{nnn} is subject to error because of the cutoff after next nearest neighbors. This error can be estimated by including the third nearest neighbor coupling J_3 and studying the allowed values of the three interaction parameters and by requiring the fulfilment of the conditions

K. I. Juntunen, K. Lefmann, T. A. Knuuttila, and J. T. Tuoriniemi

(3) and (4) above. Fig. 1 displays the allowed values of J_{nn} (solid line) and J_{nnn} (dashed line) as a function of J_3. The inset shows the less plausible family of solutions, where $|J_{nn}| < |J_{nnn}|$ for most values of J_3. As Fig. 1 demonstrates, the values of J_{nn}, J_{nnn} and J_3 are, in fact, quite uncertain, even their signs cannot be determined without further assumptions.

If we adopt the loose criterium $|J_{nn}| > |J_{nnn}| > |J_3|$, we limit the parameter space to the two J_3 intervals $-3.5...-3$ (h Hz) and $-2...2$ (h Hz). Both solutions give a value of J_{nn} of $13...16$ (h Hz), while the value of J_{nnn} varies considerably. The negative J_3 interval gives positive values of J_{nnn} of $12...3$ (h Hz), while the interval close to $J_3 = 0$ gives $J_{nnn} = -12...-2$ (h Hz). The latter interval seems more plausible since J_1 and J_2 have different signs as seen in Cu and Ag. In this work we have adopted the central value in this interval, $J_3 = 0$, giving the values of J_{nn} and J_{nnn} listed above. This choice is, in fact, a necessity for the method of exact diagonalization of small spin clusters, since the system size used in this work does not allow third-nearest neighbor interaction.

It must be noted that since the number of 3rd nearest neighbors is as high as 24 compared to 12 nearest and 6 next nearest neighbors, the contribution of a non-zero J_3 to the magnetic properties could be large even if it were small compared to J_{nn} and J_{nnn}. For example, a small negative value of J_3 would frustrate AFM type-I order.

3.   HIGH TEMPERATURE EXPANSIONS

We present here the general results of a high temperature expansion of a system with Zeeman, Heisenberg, and dipolar interactions up to 4th order in β. A similar high temperature expansion was performed already in 1937 by van Vleck [4]. However, our expressions are more general, and we have thus chosen to present them here.

The high temperature expansion of a system is performed by expanding the partition function around $\beta = 0$

$$Z = \text{tr}\{\exp(-\beta H)\} \approx \text{tr}\{1\}\left(1 + \sum_{n=1}^{\infty} \frac{(-\beta)^n}{n!}\langle H^n \rangle\right), \qquad (5)$$

where $\langle H^n \rangle$ denotes the unweighted average, $\text{tr}\{H^n\}/\text{tr}\{1\}$. The logarithm of Z is expanded as

$$\ln Z = \sum_{n=0}^{\infty} \frac{c_n}{n!}\beta^n, \qquad (6)$$
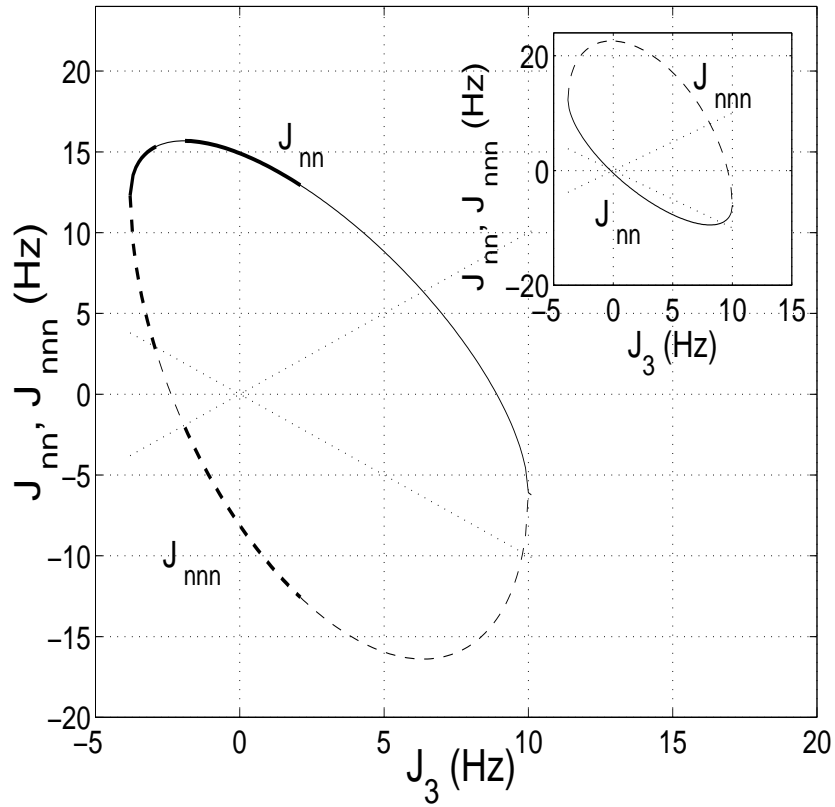
Fig. 1. The allowed values of J_{nn} (solid line) and J_{nnn} (dashed line) as a function of J_3. The inset shows the less plausible solution, and the main figure shows the more likely solution. The dotted lines indicate the condition $|J_{nn}|, |J_{nnn}| = |J_3|$. The bold parts represent the most probable solutions.

where the coefficients c_n are called cumulants. For the Hamiltonian (1), $\langle H \rangle = 0$, whence the first few cumulants become

$$c_0 = N \ln(2I + 1) \tag{7}$$

$$c_1 = 0 \tag{8}$$

$$c_2 = \left\langle H^2 \right\rangle \tag{9}$$

$$c_3 = -\left\langle H^3 \right\rangle \tag{10}$$

$$c_4 = \left\langle H^4 \right\rangle - 3 \left\langle H^2 \right\rangle^2. \tag{11}$$

The thermodynamical quantities of the system are obtained from this expansion using

$$S = \frac{\partial}{\partial T}(k_B T \ln Z) = k_B \sum_{n=0}^{\infty} \frac{c_n(1-n)}{n!} \beta^n \tag{12}$$

$$\chi = \mu_0 k_B T \frac{\partial^2 \ln Z}{\partial B^2} = \mu_0 \sum_{n=1}^{\infty} \frac{\beta^{n-1}}{n!} \frac{\partial^2 c_n}{\partial B^2} \tag{13}$$

$$p = \frac{k_B T}{I \gamma \hbar N} \frac{\partial \ln Z}{\partial B} = \frac{1}{I \gamma \hbar N} \sum_{n=1}^{\infty} \frac{\beta^{n-1}}{n!} \frac{\partial c_n}{\partial B}. \tag{14}$$

where χ is the real part of the longitudinal susceptibility and $p = \langle I^z \rangle / I$ is the polarization.

3.1.   Second order terms

In the well known second order HTE expression, all cross terms between the three terms in the interaction vanish:

$$\left\langle H^2 \right\rangle = \left\langle H_z^2 \right\rangle + \left\langle H_{RK}^2 \right\rangle + \left\langle H_d^2 \right\rangle. \tag{15}$$

The first term is

$$\left\langle H_z^2 \right\rangle = C k_B B^2, \tag{16}$$

where $C = N \gamma^2 \hbar^2 I(I + 1)/(3k_B)$ is the Curie constant. This is the term giving the high temperature free spin behavior, like the Curie susceptibility $\chi_0 = \mu_0 C/T$. The remaining part of (15) describes the spin-spin correlation, which gives the first non-trivial contribution to the zero field entropy.

$$\left\langle H_{RK}^2 \right\rangle + \left\langle H_d^2 \right\rangle = C k_B B_{loc}^2, \tag{17}$$

where the local field B_{loc} was defined in Eq. (4).

3.2. Third order terms

The complete third order HTE expression is

$$\left\langle H^3 \right\rangle = 3 \left\langle H_z^2 (H_{\mathrm{RK}} + H_{\mathrm{d}}) \right\rangle + \left\langle (H_{\mathrm{RK}} + H_{\mathrm{d}})^3 \right\rangle. \tag{18}$$

Here

$$3 \left\langle H_z^2 (H_{\mathrm{RK}} + H_{\mathrm{d}}) \right\rangle = -3Ck_{\mathrm{B}}^2 B^2 \Theta, \tag{19}$$

where the Curie-Weiss temperature Θ is defined by

$$
\begin{aligned}
\Theta &= -\frac{1}{3k_{\mathrm{B}}} I(I+1) \sum_k \left(J_{0k} + D_{0k}(1 - 3\cos^2\theta_{0k}) \right) \\
&= \frac{1}{3k_{\mathrm{B}}} I(I+1) \mu_0 \gamma_{\mathrm{eff}}^2 \hbar^2 \rho (R_{\mathrm{eff}} + L - D), \tag{20}
\end{aligned}
$$

where θ_{jk} is the angle between $\hat{r}_{jk}$ and $\mathbf{B}$, $R_{\mathrm{eff}} = R\gamma^2/\gamma_{\mathrm{eff}}^2$, $L = 1/3$ is the Lorentz factor, and D is the demagnetization factor of the sample in the direction of the magnetic field. The second term in the third order expression is

$$
\begin{aligned}
\left\langle (H_{\mathrm{RK}} + H_{\mathrm{d}})^3 \right\rangle &= \frac{I^2(I+1)^2}{12} N \sum_k \left(-J_{0k}^3 + 3J_{0k}D_{0k}^2 + 2D_{0k}^3 \right) \tag{21} \\
&+ \frac{I^3(I+1)^3}{9} N \sum_{kl} \Big[J_{0k}J_{0l}J_{kl} - 3J_{0k}D_{0l}D_{kl}(1 - 3t_{0lk}^2) \\
&+ D_{0k}D_{0l}D_{kl}[-2 + 3(t_{0kl}^2 + t_{0lk}^2 + t_{k0l}^2) + 9t_{0kl}t_{0lk}t_{k0l}] \Big],
\end{aligned}
$$

where $t_{jkl} = \cos(\phi_{jkl})$, and ϕ_{jkl} is the angle between the vectors $\hat{r}_{jk}$ and $\hat{r}_{lk}$. Here the first line is the higher order correction to the two-spin correlations, and the last two lines come from three-spin correlations, which depend on the lattice geometry.

The susceptibility calculated from the third order HTE is, in fact, a series expansion of the Curie-Weiss-law [4],

$$\chi_{\mathrm{cw}} = \mu_0 \frac{C}{T - \Theta}. \tag{22}$$

3.3. Fourth order terms

The fourth order term is written as

K. I. Juntunen, K. Lefmann, T. A. Knuuttila, and J. T. Tuoriniemi

$$\left\langle H^4 \right\rangle = \left\langle H_z^4 \right\rangle + \left\langle (H_{\mathrm{RK}} + H_{\mathrm{d}})^4 \right\rangle + \left\langle 6H_z^2 (H_{\mathrm{RK}} + H_{\mathrm{d}})^2 \right\rangle, \quad (23)$$

where the last term is an abbreviation of the 6 different permutations of its constituents; the terms do not commute. Here we present only the magnetic field dependent parts of the fourth order term. The full 4th order term will be given in Ref. 11. The term containing four Zeeman interactions is

$$\left\langle H_z^4 \right\rangle = C k_{\mathrm{B}} \gamma^2 \hbar^2 B^4 \left[N I(I+1) - (2I^2 + 2I + 1)/5 \right]. \quad (24)$$

This term represents the second non-zero contribution to the free spin magnetization: the second non-zero term in a series expansion of the Brillouin function.

The terms with two Zeeman interactions and two spin-spin interactions are

$$
\begin{aligned}
&\left\langle 6H_z^2 (H_{\mathrm{RK}} + H_{\mathrm{d}})^2 \right\rangle \quad\quad\quad\quad\quad\quad\quad\quad\quad\quad\quad (25)\\[4pt]
&= C k_{\mathrm{B}} B^2 I(I+1) \Big[N I(I+1) \sum_k J_{0k}^2 - \sum_k J_{0k}^2 \\
&+ \frac{4}{3} I(I+1) \sum_{kl} J_{0k} J_{0l} \\
&+ \frac{4}{5} (8I^2 + 8I - 1) \sum_k J_{0k} D_{0k} (1 - 3\cos^2 \theta_{0k}) \\
&+ \frac{8}{3} I(I+1) \sum_{kl} J_{kl} D_{0k} (1 - 3\cos^2 \theta_{0k}) \\
&+ 2 N I(I+1) \sum_k D_{0k}^2 - \frac{1}{5} \sum_k D_{0k}^2 (2 + 9\cos^2 \theta_{0k}) \\
&- \frac{4}{5} I(I+1) \sum_k D_{0k}^2 (1 - 3\cos^2 \theta_{0k}) \\
&+ \frac{4}{3} I(I+1) \sum_{kl} D_{0k} D_{0l} (1 - 3\cos^2 \theta_{0k} - 3\cos^2 \theta_{0l} \\
&\quad\quad\quad\quad\quad\quad\quad\quad\quad\quad + 9 t_{k0l} \cos \theta_{0k} \cos \theta_{0l}) \Big].
\end{aligned}
$$

The terms in Eqs. (24 and 25) proportional to N^2 contribute to the expansion only by cancelling the term $-3\left\langle H^2 \right\rangle^2$ in the expression for c_4, thus leaving the cumulant proportional to N.

3.4. Padé approximants

The Padé approximant method is often used to extend the region of validity of a series expansion, e.g. a HTE [12]. The central idea behind these approximants is to find a rational fraction, whose series expansion equals the original series. One choice for the Padé approximant for the 3rd order HTE of the entropy (our zero field entropy) is the (1,2) expansion

$$1 - S_{\mathrm{red}} \approx \frac{1 - \frac{2}{3}\frac{c_3}{c_2}\beta}{1 - \frac{2}{3}\frac{c_3}{c_2}\beta + \frac{c_2}{2\ln 2N}\beta^2}. \tag{26}$$

and (1,3) expansion for the 5th order HTE for entropy (our high field entropy),

$$S_{\mathrm{red}} \approx \frac{c_2}{2\ln 2}\beta^2 \frac{1 + (b_S + \frac{2}{3}\frac{c_3}{c_2})\beta}{1 + b_S\beta + (-\frac{1}{4}\frac{c_4}{c_2} - \frac{2}{3}\frac{c_3}{c_2}b_S)\beta^2}, \tag{27}$$

where

$$b_S = \frac{\frac{1}{15}\frac{c_5}{c_2} - \frac{1}{6}\frac{c_3 c_4}{c_2^2}}{\frac{4}{9}\left(\frac{c_3}{c_2}\right)^2 - \frac{1}{4}\frac{c_4}{c_2}}. \tag{28}$$

The Padé approximants for the HTE of all other thermodynamical quantities can be found in a similar way. We have chosen to use the set of approximants, with which the best fit to the exact ED data was achieved. We have used the (1,2) expansion for polarization (here $I = 1/2$),

$$p \approx \frac{\frac{1}{2}\gamma\hbar\beta B\left[1 + (k_{\mathrm{B}}\Theta + b_p)\beta\right]}{1 + b_p\beta + \left[-k_{\mathrm{B}}\Theta b_p + (\gamma^4\hbar^4 B^4/8 - c_4/N)/(3\gamma^2\hbar^2 B^2)\right]\beta^2}, \tag{29}$$

where

$$b_p = -\frac{k_{\mathrm{B}}\Theta}{3\gamma^2\hbar^2 B^2}\frac{7/8\gamma^4\hbar^4 B^4 + c_4/N}{(k_{\mathrm{B}}\Theta)^2 + (\gamma^4\hbar^4 B^4/8 - c_4/N)/(3\gamma^2\hbar^2 B^2)}. \tag{30}$$

We also use a (0,2) expansion for susceptibility,

$$\chi \approx \frac{\frac{1}{4}\mu_0\gamma^2\hbar^2\rho\beta}{1 - k_{\mathrm{B}}\Theta\beta + \left[(k_{\mathrm{B}}\Theta)^2 + (\gamma^4\hbar^4 B^4/8 + c_4/N)/(3\gamma^2\hbar^2 B^2)\right]\beta^2}. \tag{31}$$

K. I. Juntunen, K. Lefmann, T. A. Knuuttila, and J. T. Tuoriniemi

4. EXACT DIAGONALIZATION

The exact numerical diagonalisations were performed using the software package RLexact [13]. The spin Hamiltonian is made translationally invariant by applying periodic boundary conditions and broken up into block-diagonal matrices by explicit use of the symmetries of the Hamiltonian, as described in Ref. 14. The usual method for diagonalizing spin Hamiltonians is the Lanczos algorithm [15], which yields the extreme eigenvalues and eigenvectors of the spin system. However, for high-temperature thermodynamics it is necessary to obtain the full energy spectrum, whence direct matrix diagonalization methods were used. This limited the system size to $N = 16$, a size where the full fcc symmetry can be used. The next higher system size would be $N = 32$ [16], which is prohibitively large with matrix dimensions exceeding 10^7. Because of the dipolar couplings, the magnetisation along the field direction is not a good quantum number, in contrast to pure Heisenberg systems. All in all, the largest matrix dimension is 4156. A complete calculation for each field value involved diagonalization of three matrices of this size. The computation time on a 500 MHz Pentium II PC was 21 hours per matrix, but for most of the calculations a faster IBM SP computer has been used. The output of the program was for each eigenstate, $|\phi_j\rangle$, the energy, E_j, and the magnetisation along the field direction, $m_i = \sum_i \langle \phi_j | s_i^z | \phi_j \rangle$.

In the calculations we have aimed at using the values of J_{nn}, J_{nnn}, D_{nn}, and D_{nnn} calculated for Rh. However, since for each spin there are only 3 different nnn in the $N = 16$ cluster, as compared to 6 in the infinite system, we must adjust the nnn couplings. A mean-field like approach would be to multiply J_{nnn} and D_{nnn} by 2, which would cause the RK parameter R and the Curie-Weiss temperature, Θ, to remain unchanged. This, however, would cause wrong values of the HTE already in the 2nd order term, as the interactions occur squared in B_{loc}. To reach the correct value of B_{loc}, we hence multiply only with $\sqrt{2}$ [8].

In the pure nearest neighbor Heisenberg $N = 16$ system with periodic boundary conditions, the energy gap between the (5 times degenerate) ground state and the lowest excited state has the value J_{nn}. However, the dipolar interaction lifts the ground state degeneracy to form a series of excited states which resemble a continuum. In the present work, the gap from the (non-degenerate) ground state to the first excited level (doubly degenerate) is 1.5 (h Hz) with a further gap of 6 (h Hz) to the second lowest excited state(s). In general, the splitting between the lowest levels is of the order 2-4 (h Hz), which corresponds to 0.1-0.2 (k_{B} nK). We could thus expect our exact diagonalisations not to show finite-size artefacts down to temperatures above ~ 0.2 nK.

Exact diagonalization of the rhodium nuclear spin system

The general results of the HTE from the previous section were applied to the $N = 16$ system with periodic boundary conditions. These calculations were checked against the ED results directly, since $\text{tr}\{H^n\} = \sum_j E_j^n$ can be calculated directly. In all cases, the relative agreement was better than 10^{-3}.

5. RESULTS AND DISCUSSION

In this chapter we present results for the ED, HTE and Padé approximant calculations on Rh. The results are compared with experimental data; the experimental details of obtaining the data can be found in Ref. 1. The HTE for the finite size system is included in the figures in order to give an idea of how the HTE deviates from the behavior of an exact solution, and it also gives a reference, down to which temperatures the HTE for the infinite system is reliable. Also, compared to the HTE for the infinite system, it demonstrates to which extent the ED suffers from finite size effects.

In calculating the HTE results, the total high temperature expansions have been included up to third order and the B^2-dependent terms up to 4th order. For the study of the system in high fields, we have included the B^4-dependent terms of the fifth order expression. The rhodium sample used in the measurements had a demagnetization factor $D = 0.08$ in the direction of the external field, and this value has been used in the corresponding infinite lattice HTE calculations.

In calculating the sums with RK interactions, cutoff after nnn of the RK interaction was assumed. The sums in Eqs. (4), (21) and (25) containing dipolar interactions were extended far enough to assure convergence. Surface effects were assumed to be negligible.

5.1. High field entropy

At high magnetic fields, the polarization of a spin system is proportional to the area of the NMR peak, which can be directly measured. The reduced entropy of the nuclear spin system is calculated from nuclear polarization using the combinatoric relation [2]

$$
\begin{aligned}
S_{\text{red}} &= 1 - S/(k_{\text{B}} N \ln 2) \\
&= \left[(1 + p)\ln(1 + p) + (1 - p)\ln(1 - p)\right]/(2 \ln 2) \quad (32)
\end{aligned}
$$

for $I = 1/2$. This relation is exact for an infinite system of non-interacting spins. Fig. 2 shows the reduced entropy of the Rh nuclear spin system as a function of polarization at a field of $\approx 320\ \mu$T, which was the experimentally

used field value for Rh. The figure shows the free spin results, the results of ED, HTE, and Padé on an $N = 16$ cluster, and HTE and Padé results for the infinite lattice. The entropy and polarization for the HTE have been calculated by using Eqs. (12) and (14) for a specific temperature and then eliminating the temperature. As seen in Fig. 2, the high field entropy of the ED system agrees well with that of the free-spin system. This is remarkable, since the ED system is neither infinite nor contains free spins. The maximum deviation between the two is approximately 0.1%. Also the HTE's of both the finite and the infinite system agree with the free spin expression up to $p \approx 0.5$, and the respective Padé expressions agree up to $p \approx 0.6$. As $S_{\mathrm{red}} \to 1$ as $p \to 1$, we can verify the free spin result as a very good approximation for all values of p. Thus, the frequent use of Eq. (32) by experimentalists is well justified. Further, this result shows clearly the weakness of the HTE at high polarizations (low temperatures). the region of validity of the HTE.

5.2. Zero field entropy

Figure 3 shows the zero field entropy of the Rh spin system as a function of temperature. As the figure demonstrates, all methods accurately describe the entropy of the real system in the paramagnetic state above ≈ 5 nK. In the figure it is seen that the HTE for the infinite lattice agrees well with the experimental data before it diverges at ≈ 2 nK, whereas the Padé approximant agrees down to ≈ 1 nK and shows no divergence. The Padé approximant for the finite-size system agrees with the ED result down to ≈ 2 nK, and deviates considerably from it only below ≈ 0.5 nK. The HTE for the finite size system is monotonic on the scale of this figure, and it deviates at a similar temperature than the HTE for the infinite system.

The reason for the difference between the HTE's lies in the magnitude of the third order term of HTE at zero field: the infinite system has $\langle H^3 \rangle = 15000N(h\ \mathrm{Hz})^3$, whereas the finite-size system has $\langle H^3 \rangle = 1200N(h\ \mathrm{Hz})^3$, and the pure Heisenberg nnn model has $\langle H^3 \rangle = -300N(h\ \mathrm{Hz})^3$. A positive value of $\langle H^3 \rangle$ indicates that frustration is present in the system, while a negative value indicates the absence of it. At temperatures below ≈ 5 nK, the ED system has a lower entropy per spin than the infinite system. This is due to the fact that the long range dipolar forces increase entropy, as can be deduced by considering the above magnitudes of $\langle H^3 \rangle$ for different models.

At temperatures below 1 nK, the experimental points show much higher entropies than any of the calculational approaches. The reason for this is not understood, but the high experimental entropy value goes well along with
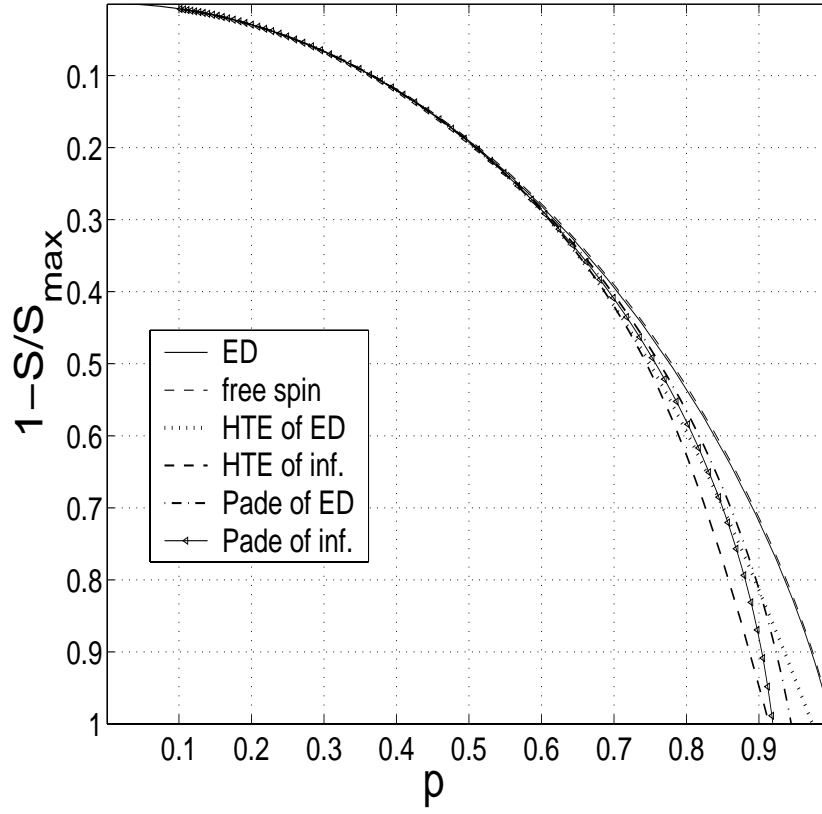
Fig. 2. Reduced entropy vs. polarization for Rh nuclei in an external field $B \approx 320 \ \mu$T. Solid line is the ED result, and the almost invisible dashed line under it is the free-spin entropy from Eq. (32). The dotted line is the HTE result for the finite-size system, and the dashed line is the HTE for the infinite system. The dash-dotted line is the Padé approximant for the HTE of the finite size system and the solid line with triangles is the same for infinite lattice HTE. The HTEs include the B^4 dependent terms up to fifth order, the B^2 dependent terms up to fourth order, and the total terms up to third order.

K. I. Juntunen, K. Lefmann, T. A. Knuuttila, and J. T. Tuoriniemi
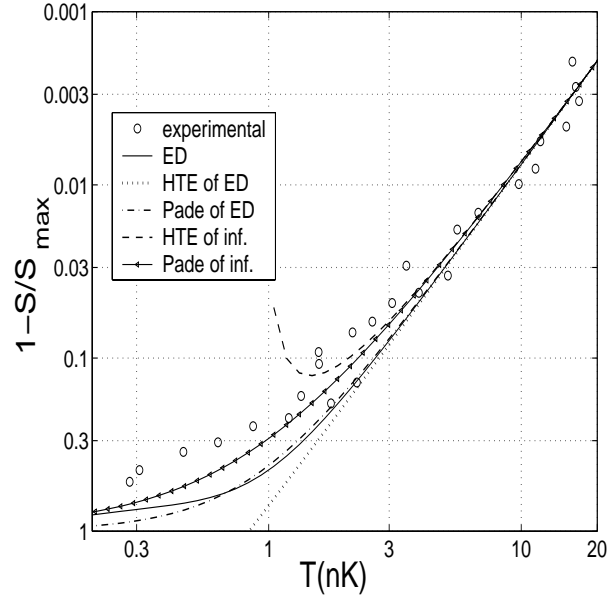
Fig. 3. Reduced entropy vs. nuclear temperature in zero field shown in a log-log plot. The dots represent the experimental data.

the absence of order in the system.

5.3. Polarization–temperature relation

In nuclear magnetism experiments, the temperature of the spin system may be measured directly only by the elaborate way of using the second law of thermodynamics, by a) measuring the initial entropy S_i in magnetic field b) applying a known heat pulse ΔQ in zero magnetic field and c) measuring the final entropy S_f in magnetic field. Then $T = \Delta Q/(S_f - S_i)$, since the field changes are performed adiabatically [1]. The entropy is calculated from polarization measurements at high fields using Eq. (32). A practical way of determining the temperature is to use a measurement of the high field polarization and then convert this to the corresponding temperature after a subsequent adiabatic demagnetisation to zero field. A second order expansion of both high-field and zero field entropy would give $p^2 = (bT)^{-2}$, while a more accurate semiempirical formula has been applied [17]:

$$|1/p| = 1 + b|T|, \tag{33}$$

where $b = 2k_B/(\gamma\hbar B_{loc}) = 0.94$ nK^{-1} for rhodium.

Exact diagonalization of the rhodium nuclear spin system

In Fig. 4, the ED, HTE and Padé results for high field $1/p$ as a function of low field temperature are shown, and the results are compared with experimental data. For the HTE and ED results, the temperatures have been calculated by first finding the entropy corresponding to the high field polarization, using Eq. (32), and then finding the temperature on the zero field entropy curve, in Fig. 3, with the same entropy value. In the figure, the HTE for the infinite system ends at approximately 2 nK, where the HTE entropy has a minimum, see Fig. 3.

The ED and HTE for the infinite lattice have slightly different local fields, because for the ED system there exists nnn cutoff for the dipolar interaction. Since the relationship between p and T is sensitive to the local field, the $1/p$ vs. T results for ED and the HTE for the infinite system do not agree even at high temperatures. However, the difference is small, and all results in Fig. 4 have approximately the same slope, but different offsets, at high temperatures. Due to the scatter in the data, it is difficult to judge which one of the infinite lattice HTE or the semiempirical straight line best describes the experimental data at high temperatures.

The exact diagonalization result does not support the linear semiempirical formula (33) and does not agree with the experimental data either. However, the exact diagonalization result is expected to deviate from the real behavior due to finite-size effects. The HTE for the infinite lattice is seen to deviate less than the ED result from the semiempirical law. Since, as basic thermodynamics implies, $p \to 1$ for $T \to 0$, the behavior of the infinite lattice is obviously much less nonlinear than the behavior of the ED result. No more information is gained from the Padé approximants which seem to be of little use for the temperature-polarization relation. Below ~ 1 nK, only the semiempirical formula agrees with the data. This fact is related to the low-temperature discrepancy of the entropy shown in Fig. 3 and cannot be explained by this work.

5.4. Zero field susceptibility

A standard way of searching for nuclear magnetic ordering is to measure the static susceptibility, since ordering should produce a noticeable change in its behavior. Fig. 5 displays the zero field susceptibility vs. the high field polarization. The ED susceptibility has been calculated using $\chi = \mu_0 \Delta M / \Delta B$ for a small ΔB. The ED result is seen to exhibit the same kind of bending behavior at high polarizations as the experimental data, even though there is a considerable difference in the magnitudes of these quantities at high polarizations. Since the nnn parameters are adjusted by
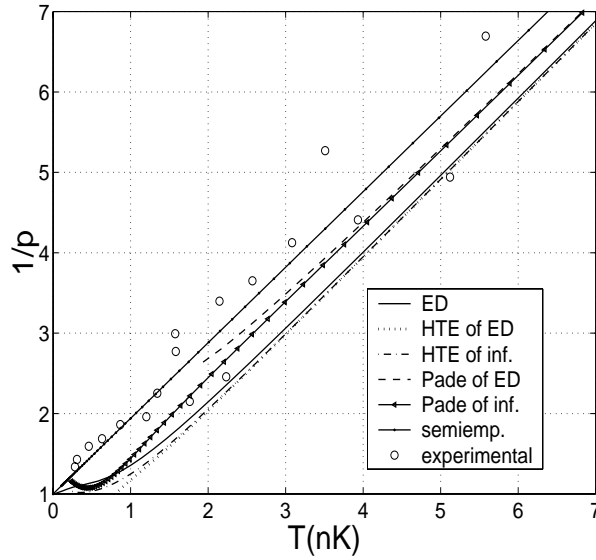
Fig. 4. Inverse high field polarization vs. nuclear temperature after an adiabatic demagnetisation to zero field. Straight solid line is the semiempirical law (33).

$\sqrt{2}$ for the ED, the Curie-Weiss temperature Θ for the ED differs from that for the infinite lattice, and thus the ED result has a lower susceptibility than the Curie-Weiss law indicates. At small polarizations the ED and the HTE for the infinite lattice agree, as they should, but there is a small offset in the experimental data, which is not understood.

Fig. 6 displays the inverse static susceptibility as a function of temperature. The figure displays the ED result, the HTE for the finite size system and infinite lattice, and the Curie-Weiss result (22), for which the values $\mu_0 C/V = 1.3$ nK, and $\Theta = -1.18$ nK have been used. The experimental data shown in Figs. 5 and 6 are obtained from different runs.

The Padé approximant is seen to extend the validity of the HTE for the finite size system considerably in this figure, from ~ 5 nK to ~ 1.5 nK. The infinite lattice result agrees quite well with the experimental data at the low temperature end; the Padé approximant agrees even down to ≈ 0.5 nK.

6. CONCLUSIONS

We have performed exact diagonalization and high temperature expansion calculations of the entropy, polarization and susceptibility. Our ED and
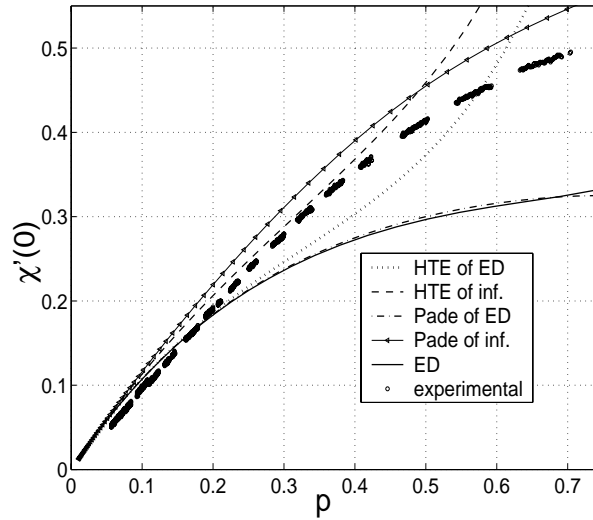
Fig. 5. Static susceptibility vs. nuclear polarization.
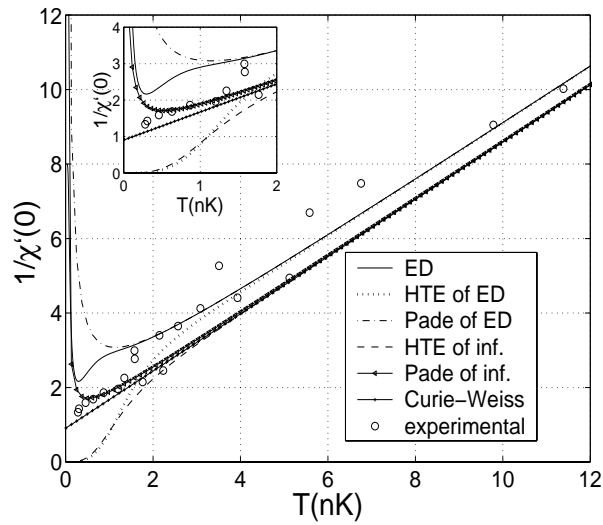
Fig. 6. Inverse static susceptibility vs. nuclear temperature. The straight solid line is the Curie-Weiss result. The insert shows a magnification of the low temperature end of the figure. The experimental data in this figure come from a different run than in Fig. 5

K. I. Juntunen, K. Lefmann, T. A. Knuuttila, and J. T. Tuoriniemi

HTE results fit in general well to the experimental data at high temperatures. Further, the HTE for the infinite lattice agrees well with the experimental data at all temperatures of its validity, except for an offset in the susceptibility, which is most probably of experimental origin. Because of this good agreement, we conclude that our calculation of the interaction parameters is a fairly good approximation, even though there is inaccuracy in their determination. The ED method deviates from the real behavior, especially for the entropy and polarization, at medium and very low temperatures, but shows the correct general tendencies.

With the Padé approximant method, the divergence of the HTE was removed and the discrepancies were lowered considerably. This is important for our work, since the interesting physics of the Rh spin system occurs at the very low temperature region, where the normal HTE would give no reasonable results. The Padé approximants for the finite system fit well to the ED data down to ≈ 1 nK, and therefore we expect the Padé approximant method to describe also the infinite lattice down to approximately those temperatures. This is also seen to be in agreement with the experimental data. At high fields, we believe that at the highest polarizations, the ED result best describes the real behavior, since it agrees well with the free spin expression, which is a good approximation at high fields. Also, it is the only expression that obeys $S \to 0$ as $p \to 1$.

All in all, we seem to have described the Rh nuclear spin system quite well in the paramagnetic state down to ~ 1 nK. Since the agreement with the experimental data is good, the use of our methodology can be expected to be justified in predicting the thermodynamics also for systems with no experimental data available. On the basis of our calculations, we cannot state definitely whether the finite size system shows signs of magnetic ordering at very low temperatures. Our next task will be to calculate the structure factors, which will hopefully give some more information on the problem of the absence of ordering in rhodium.

Exact diagonalization of the rhodium nuclear spin system

REFERENCES

1. T. A. Knuuttila, J. T. Tuoriniemi, K. Lefmann, K. I. Juntunen, F. B. Rasmussen, and K. K. Nummila, to appear in *J. Low Temp. Phys.* (2001).
2. A. S. Oja and O. V. Lounasmaa, *Rev. Mod. Phys.* **69**, 1 (1997).
3. H. E. Stanley, *Introduction to Phase Transitions and Critical Phenomena*, Clarendon Press, Oxford 1971.
4. J. H. van Vleck, *J. Chem. Phys.* **5**, 320 (1937).
5. J. C. Bonner and M. E. Fischer, *Phys. Rev. A* **135**, 640 (1964).
6. D. D. Betts and J. Oitmaa, *Phys. Lett.* **62A**, 277 (1978); J. Oitmaa, D. D. Betts, *Can. J. Phys.* **56**, 897 (1978).
7. M. C. Cross and R. N. Bhatt, *J. Low Temp. Phys.* **57**, 573 (1984).
8. K. Lefmann, J. Ipsen, and F. B. Rasmussen, *Physica B* **284**, 1702 (2000).
9. J. T. Tuoriniemi, T. A. Knuuttila, K. Lefmann, K. K. Nummila, W. Yao, and F. B. Rasmussen, *Phys. Rev. Lett.* **84**, 370 (2000).
10. P. A. Lindgård, X. -W. Wang, and B. N. Harmon, *J. Magn. Magn. Mater.* **54-57**, 1052 (1986); S. J. Frisken, and D. J. Miller, *Phys. Rev. Lett.* **57**, 2971 (1986); D. J. Miller, and S. J. Frisken, *J. Appl. Phys.* **64**, 5630 (1988); B. N. Harmon, X. -W. Wang, and P. A. Lindgård, *J. Magn. Magn. Mater.* **104-107**, 2113 (1992).
11. K. Lefmann and K. I. Juntunen, *Low Temperature Laboratory Report*, to be published (2001).
12. *Phase Transitions and Critical Phenomena* vol. 3, edited by C. Domb and M. S. Green, Academic Press (1974).
13. C. Rischel and K. Lefmann, to be published.
14. K. Lefmann and C. Rischel, *Phys. Rev. B* **54**, 6340 (1996).
15. C. Lanczos, *J. Res. Nat. Bur. Standards, Sect. B*, **45**, 255 (1950).
16. K. Lefmann and C. Rischel, to appear in *Europ. Phys. J.* B (2001).
17. P. J. Hakonen and S. Yin, *J. Low Temp. Phys.* **85**, *25 (1991)*.